Soft Matter

Accepted Manuscript

ROYAL SOCIETY OF CHEMISTRY

www.rsc.org/softmatter

Soft Matter

RSCPublishing

ARTICLE

Kinetics of Domains Registration in Multicomponent Lipid Bilayer Membranes

Cite this: DOI: 10.1039/x0xx00000x

Kan Sornbundit,[a,b] Charin Modchang,[b] Wannapong Triampo, [a,b] Darapond Triampo,[c] Narin Nuttavut,[b] P.B Sunil Kumar [e,f] and Mohamed Laradji *[a,f]

Received 14th May 2014,

DOI: 10.1039/x0xx00000x

www.rsc.org/softmatter

The kinetics of registration of lipid domains in the apposing leaflets of symmetric bilayer membranes is investigated via systematic dissipative particle dynamics simulations. The decay of the distance between the centres of mass of the domains in the apposing leaflets is almost linear during early stages, and then becomes exponential during late times. The time scales of both linear and exponential decays are found to increase with decreasing the strength of interleaflet coupling. The ratio between the time scales of the exponential and linear regimes decreases with increasing the domain size, implying that the decay of the distance between the domains centres of mass is essentially linear for large domains. These numerical results are largely in agreement with the recent theoretical predictions of Han and Haataja [Soft Matter (2013) 9:2120-2124]. We also found that the domains become elongated during the registration process.

1 Introduction

Many in-vitro experiments of multicomponent giant unilamellar lipid vesicles and supported bilayers have shown that these systems exhibit interesting lateral inhomogeneities in the form of liquid ordered domains, rich in cholesterol and saturated lipids, coexisting with liquid disordered domains rich in unsaturated lipids [1-9]. The understanding of domain formation in lipid membranes is particularly relevant to the lateral organization of plasma membranes of eukaryotic cells, which are inherently multi-component. Indeed, there currently exists a consensus that the plasma membrane of mammalian cells, in particular, exhibits nanscale domains, known as lipid rafts, which are rich in sphingomyelin and cholesterol [10-12]. Lipid rafts are involved in many cellular processes such as signalling, trafficking, and endocytosis.

An intriguing feature of phase-separating lipid membranes is that domains in the two leaflets exhibit almost complete registration, i.e., domains in the outer leaflet almost exactly co-localise with domains in the inner leaflet [1-9]. Collins and Keller [12] demonstrated that lipid membranes with asymmetric transbilayer lipid composition exhibit phase separation with registration even if one of the two leaflets would not exhibit phase separation by itself. This experiment suggests that there exist some coupling between the two apposing leaflets of the bilayer that drives domains co-localization. May proposed earlier that the interleaflet coupling might result from chain interdigitation, electrostatic coupling, or rapid cholesterol flip-flop, with chain interdigitation probably being the main contributor to domains registration [13,14]. The transbilayer lipid distribution in the plasma membrane is inherently asymmetric [15]. In fact, the outer leaflet of the plasma membrane is composed of sphingolipids, phosphatidylcholine and cholesterol, while the cytoplasmic leaflet is mainly composed of phosphatdylethanolamine, phosphatdylserine, and cholesterol. Experiments have shown that bilayers composed of lipids with composition similar to that of the outer leaflet exhibit phase separation, while bilayers with composition similar to that of the inner leaflet do not exhibit phase separation [16]. A coupling between the two leaflets of the plasma membrane implies that lipid rafts in the outer leaflet would also lead to rafts in the cytoplasmic leaflet. The colocalization of rafts in both leaflets may be necessary for signal transduction across the bilayer [17].

The kinetics of phase separation in multicomponent lipid membranes has been the subject of many experimental, theoretical and computational studies during the last decade [6-8,18-24]. Interleaflet coupling is typically assumed in the theoretical and computational studies. Consequently, domain registration is observed since the inception of the phase separation process [26]. However, while these studies have provided valuable understanding of the mechanisms and details

of phase separation in multicomponent lipid bilayers, our understanding of how domains undergo registration in the first place during the early stages of the phase separation process is not well understood.

So far, experimental studies investigating the kinetics of domain registration in multicomponent membranes are lacking and might be very difficult to perform. Pantano *et. al.* recently investigated these kinetics using molecular dynamics simulations of a coarse-grained lipid model of self-assembled bilayers composed of short diblock copolymer [27]. They found that registration is mainly driven by mismatch in the thickness of the coexisting phases, leading to curvature modulation [27]. More recently, Han and Haataja [28] theoretically investigated the problem based on the sharp-interface limit analysis of a generalized time-dependent Ginzburg-Landau model for the two leaflets with an interleaflet coupling [29,30]. For the sake of tractability of the analyses, domains are assumed circular, without out-of-plane fluctatuations. The effect of the ambient solvent is implicit, and only the membrane viscosity is taken into account in this theory. They were able to derive analytical solutions for the distance between the centres of mass of two initially partially overlapping circular domains.

Here, we present results of a systematic investigation of the kinetics of domains registration in lipid bilayers with explicit solvent using systematic dissipative particle dynamics (DPD) simulations [31-33]. This approach allows us to computationally investigate the kinetics of domain registration in bilayers while accounting for solvent effects, domain shape changes and out-of-plane fluctuations. We introduce a simple relation for systemically adjusting the coupling strength between the two leaflets in the simulations. We specifically investigated (i) the relation between the relaxation time and domain size, (ii) the relation between the relaxation time and the coupling strength, (iii) effect of initial separation distance between the two domains, and (iv) shape deformation during the registration kinetics.

The rest of this article is organized as follows: The model and method are presented in Sec. 2. The results are presented and discussed in Sec. 3. Finally, our findings are summarized in Sec. 4.

2 Model and method

Various coarse-grained models for multicomponent membranes have been used in the past [26]. The present study is based on DPD, a powerful method that has been previously used for studies of the phase separation dynamics in lipid membranes [18-21]. In the DPD approach for self-assembled membranes, a lipid molecule is modelled as a flexible amphiphilic chain with one hydrophilic (*h*) bead, mimicking the lipid head group, and a chain of three hydrophobic (*t*) beads, mimicking the lipid hydrocarbon groups. Although our lipid model is simpler than that used by Pantano *et al.* [27], we are able to investigate much larger systems over longer times and perform a more systematic study investigating the kinetics of registration of lipid domains.

In the DPD framework [31-34], beads *i* and *j*, with respective positions and velocities ($\mathbf{r}_i$,$\mathbf{v}_i$) and ($\mathbf{r}_j$,$\mathbf{v}_j$) interact via pairwise conservative, $\mathbf{F}_{ij}^{(C)}$, dissipative, $\mathbf{F}_{ij}^{(D)}$, and random forces, $\mathbf{F}_{ii}^{(R)}$, respectively given by

$$\mathbf{F}_{ij}^{(C)} = a_{\nu_i \mu_j}\omega(r_{ij})\hat{\mathbf{r}}_{ij}, \tag{1}$$

$$\mathbf{F}_{ij}^{(D)} = \gamma_{ij}\omega^2(r_{ij})(\hat{\mathbf{r}}_{ij}\cdot\mathbf{v}_{ij})\hat{\mathbf{r}}_{ij}, \tag{2}$$

$$\mathbf{F}_{ij}^{(R)} = \frac{\sigma_{ij}}{(\delta t)^{1/2}}\omega(r_{ij})\theta_{ij}\hat{\mathbf{r}}_{ij}, \tag{3}$$

where $\mathbf{r}_{ij} = \mathbf{r}_j - \mathbf{r}_i$, $\hat{\mathbf{r}}_{ij} = \mathbf{r}_{ij}/r_{ij}$ and $\mathbf{v}_{ij} = \mathbf{v}_j - \mathbf{v}_i$, δt is the time step, and the coefficients of the dissipative and random forces are interrelated through the fluctuation-dissipation theorem, $\gamma_{ij} = \sigma_{ij}/k_B T$, where T is temperature and k_B is the Boltzmann constant. In Eq. (1), ν_i and μ_j are the types of particles *i* and *j*, respectively. In the random force, Eq. (3), θ_{ij} is a symmetric random variable satisfying

$$\langle\theta_{ij}(t)\rangle = 0, \tag{4}$$

$$\langle\theta_{ij}(t)\theta_{kl}(t')\rangle = (\delta_{ik}\delta_{jl} + \delta_{il}\delta_{jk})\delta(t-t'), \tag{5}$$

with $i \neq j$ and $k \neq l$.

In Eqs. (1-3), the weight function $\omega(r)$ is given by

$$\omega(r) = \begin{cases} 1 - r/r_C & \text{for} \quad r \le r_C, \\ 0 & \text{for} \quad r > r_C, \end{cases} \tag{6}$$

where r_c is the interaction cutoff length and is used in our simulations to set the length scale of the system. Note that the same weight function is used here for the conservative and dissipative/random forces. To ensure chain connectivity, consecutive beads in a single lipid chain interact via a harmonic force,

$$\mathbf{F}_{i,i+1}^{(S)} = -C(1 - r_{i,i+1}/b)\hat{\mathbf{r}}_{i,i+1}. \tag{7}$$

The equations of motion of a bead *i* are given by

$$\frac{d}{dt}\mathbf{r}_i(t) = \mathbf{v}_i(t), \tag{8}$$

$$\frac{d}{dt}\mathbf{v}_i(t) = \frac{1}{m_i}\sum_j \left(\mathbf{F}_{ij}^{(C)} + \mathbf{F}_{ij}^{(S)} + \mathbf{F}_{ij}^{(D)} + \mathbf{F}_{ij}^{(R)}\right) \tag{9}$$

where m_i is its mass, and we assume in the present study that all DPD particles have the same mass *m*.

The present lipid model produces thermodynamically stable self-assembled lipid bilayers with mechanical and dynamical properties that are in line with experiments [35]. The same lipid model composed of two different types of lipids (*A* and *B*) is able to produce a coexistence of two liquid phases [18-21]. The two phases may be seen as coexisting liquid-ordered and liquid-disordered phases in membranes composed of a saturated lipid, an unsaturated lipid and cholesterol. The hydrophilic beads of lipids *A* and *B* are denoted by h_A and h_B, and their tail beads are denoted by t_A and t_B, respectively. Water molecules are coarse-grained into DPD beads, denoted by *w*. The values of the coefficient a_{ij} of the conservative forces, in Eq. (1), depend on the types of the interacting beads and are given by the following

$$a_{\alpha\beta} = \frac{\varepsilon}{r_C} \begin{array}{c} \\ h_A \\ t_A \\ w \\ h_B \\ t_B \end{array} \begin{array}{c} \begin{array}{ccccc} h_A & t_A & w & h_B & t_B \end{array} \\ \begin{bmatrix} 25 & 200 & 25 & 50 & 200 \\ 200 & 25 & 200 & 200 & a_{t_A t_B} \\ 25 & 200 & 25 & 25 & 200 \\ 50 & 200 & 25 & 25 & 200 \\ 200 & a_{t_A t_B} & 200 & 200 & 25 \end{bmatrix} \end{array}, \quad (10)$$

where ε is an energy scale. The interaction between tail beads of A lipids and B lipids is represented by $a_{t_A t_B}$. In previous DPD studies of multicomponent lipid bilayers [20,21], the value of $a_{t_A t_B}$ for lipids belonging to the same leaflet and that for lipids belonging to apposing leaflets were assumed to be equal [18-21]. In the present study, however, the effect of interleaflet coupling strength will be systematically studied by adjusting the interaction coefficient, $a^{\perp}_{t_A t_B}$, for hydrophobic beads belonging to apposing leaflets, with respect to the interaction coefficient, $a^{//}_{t_A t_B}$, for hydrophobic beads belonging to the same leaflet. In particular, we introduce a dimensionless coupling parameter, β, to tune the interleaflet interaction between tail beads (see Fig. 1):

$$a^{\perp}_{t_A t_B} = \beta a^{//}_{t_A t_B} + (1-\beta) a_{t_A t_A}, \quad (11)$$

with $a^{//}_{t_A t_B} = a_{t_A t_B}$ given in Eq. (10). We also assume that

$$a^{\perp}_{t_A t_A} = a^{\perp}_{t_B t_B} = a^{//}_{t_A t_A} = a^{//}_{t_B t_B} = a_{t_A t_A} = a_{t_B t_B}.$$

In Eq. (11), β=1 leads to $a^{\perp}_{t_A t_B} = a^{//}_{t_A t_B}$, which corresponds to a maximum interleaflet coupling, whereas β=0 leads to $a^{\perp}_{t_A t_B} = a_{t_A t_A} = a_{t_B t_B}$ which corresponds to no interleaflet coupling. In the later case (β=0), an A-tail bead in one leaflet does not distinguish between an A- and a B-tail bead in the apposing leaflet.

Simulations were performed at $k_B T = \varepsilon$ and a fluid density $\rho = 3.0 r_c^{-3}$. The coefficient of the random force $\sigma_{ij} = \sigma = 3.0(\varepsilon m / r_c^2)^{1/4}$ and is the same for all interacting pairs. The equations of motion were integrated using the velocity-Verlet algorithm [36,37] with a timestep, $\delta t = 0.025\tau$ where the time scale $\tau = (m r_c^2/\varepsilon)^{1/2}$. We considered three different system sizes, with periodic boundary conditions along the three axes, corresponding to $(60\times60\times40) r_c^3$, $(90\times90\times40) r_c^3$, and $(125\times125\times40) r_c^3$, depending on the size of the lipid domains. These three system sizes correspond to lipid bilayers composed of 9 000, 20 250 and 39 062 lipid molecules, respectively. The lipid domains radii that we considered range from $15 r_c$ to $40 r_c$. These three system sizes correspond to lipid bilayers composed of 9 000, 20 250 and 39 062 lipid molecules, respectively. The lipid domains radii that we considered range from $15 r_c$ to $40 r_c$.

The simulations were performed by initially preparing a one-component bilayer, composed of A-lipids, embedded in solvent beads and parallel to the xy-plane at height $z = L_z/2$. The system is then allowed to equilibrate for $t = 10^4 \tau$. Partially overlapping circular domains with equal radii, are then created by switching all A-lipids into B-lipids within partially overlapping regions, of equal radius, R, in the two apposing leaflets.

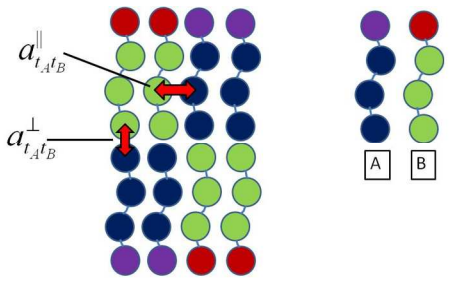

Fig. 1 (Left) Illustration of a small portion of the bilayer, indicating the interaction amplitudes between tail beads, of $a^{//}_{t_A t_B}$ and $a^{\perp}_{t_A t_B}$ used in Eq. (11). (Right) shows an illustration of the coarse-grained A and B lipids.

To quantify the kinetics of domains registration, we use the distance between the centers of mass (CM) of the two domains in the apposing leaflets,

$$\Delta h = \left[\left(x_{top} - x_{bot} \right)^2 + \left(y_{top} - y_{bot} \right)^2 \right]^{1/2}, \quad (12)$$

Where (x_{top}, y_{top}) and (x_{bot}, y_{bot}) are the coordinates of the CM of the top and bottom domains, respectively.

Recognizing that finite size effects may have an impact on the kinetics of domain growth, we performed several simulations for different domain and system sizes. We namely performed simulations for values of the ratio $r = L_x/2R$ ranging between 2 and 5, and found that finite size effects are absent.

3 Results and discussion

In this section, we present results pertinent to the (1) effect of domain size on the registration process, (2) effect of the initial separation between domains, (3) effect of interleaflet coupling on the registration kinetics, and finally (4) the anisotropy of domains during the registration process.

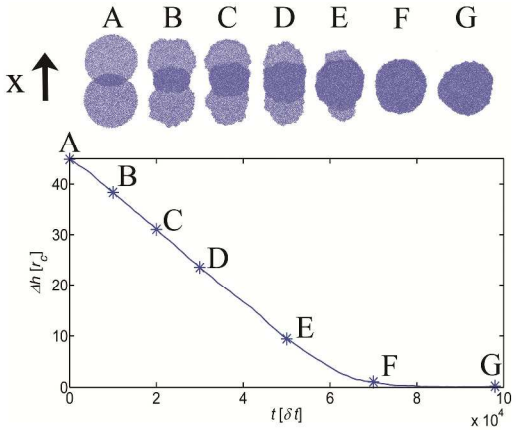

Fig. 2 (Top) Snapshot series of two domains undergoing registration along the x-axis for the case of $R = 30 r_c$, $\Delta h(0) = 1.5R$, and β=1, Lighter regions are non-overlapping while the darker regions are overlapping. (Bottom) The distance between the centres of mass of the domains vs. time.

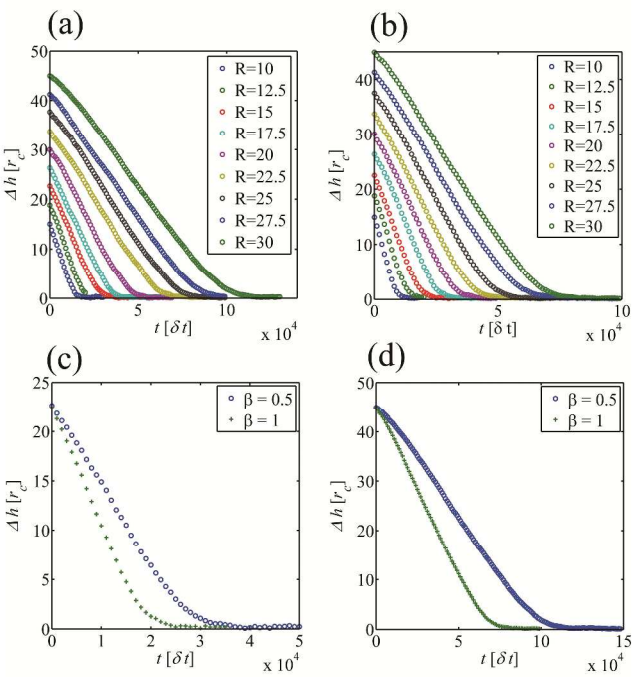

Fig. 3 (a and b) Distance between the centers of mass of the two domains, Δh , vs. time for domain radii varying between $10r_c$ ands $30r_c$. (a) and (b) correspond to coupling constants β=1 and 0.5, respectively. (c) and (d) show Δh vs. time for R=15r_c and 30 r_c, respectively. All graphs correspond to an initial separation $\Delta h(0)$=1.5R.

3.1 Effects of domain size on the registration process

Here, results are presented for the case where the domains centers of mass in the apposing leaflets are initially separated by $\Delta h(0)$=1.5R. A sequence of snapshots for the case of R=30r_c and β=1, shown in Fig 2, demonstrates qualitatively that the apposing domains move towards each other in order to complete registration. It is interesting to note that during the registration process, the domains boundaries are considerably rough and the domains become elongated along the x-axis (snapshots B-E). Eventually, during the late stages of the process, the two domains regain their circular shape (snapshots F and G). Domains anisotropy during the registration kinetics will be discussed later in more details.

In Fig. 3, Δh versus time is shown for domain radius varying between $10r_c$ and $30r_c$ and for β=0.5 and 1. Fig. 3(a-b) shows that the registration timescale increases with increasing domain size. However, the rate of registration (slope of Δh vs. time) seems to decrease with increasing the domain size. Fig. 3(c-d) shows that the registration rate increases with increasing the coupling strength β. Fig. 3 also shows that in all cases, Δh decreases with time linearly during most of the registration process.

A quantitative comparison of Δh vs. time, from our simulations, is made with the recent theoretical prediction of Han and Haataja [28]:

$$\Delta h(t) = 2R\sin\left[\arcsin\left(\frac{\Delta h(0)}{2R}\right)\left(1-\frac{t}{\tau_1}\right)\right], \qquad (13)$$

with the registration time, $\tau \sim R^2/\Lambda$, and where Λ is the interleaflet coupling parameter which is proportional to β as will be shown in Sec. 3.3. Eq. (13) is derived using sharp-interface limit analyses of a generalized time-dependent Ginzburg-Landau model for the two leaflets with an interleaflet coupling while accounting for in-plane hydrodynamics. The treatment of Ref. [28] assumes that the apposing domains must have some overlap initially. Unless the initial distance between the domains is about 2R, the decay of $\Delta h(t)$ with time is almost linear, as depicted by the solid green line in Fig. 4.

While Eq. (13) predicts that full registration is reached when $t=\tau_1$, our simulation results show that $\Delta h(t)$ crosses-over from a regime described by Eq. (13) to a slow exponential regime before τ_1 is reached, as indicated by Fig. 4. We note the excellent agreement between our results and Han-Haataja's prediction during the first regime despite that domain in the simulation are highly deformed during the kinetics, while Han-Haataja's theory assumes that the domains remain circular. We note that Pantano *et al.* [27] also observed a (nearly) linear decay of Δh with time, in their molecular dynamics simulations. The inset of Fig. 4 shows that the second stage of the registration kinetics is indeed exponential,

$$\Delta h(t) = \Delta h(\tau_1)\exp\left[-(t-\tau_1)/\tau_2\right] \qquad (14)$$

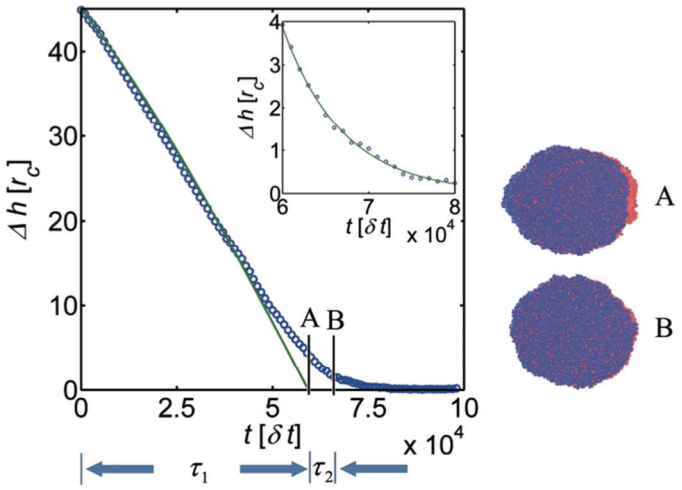

Fig. 4 Δh vs. time for the case of R=30r_c, $\Delta h(0)$=1.5R, andβ=1. Green solid line corresponds to a fit of the data with Eq. (13) during early times. The graph shows how the time scale τ_1 is extracted from the data. The late stage time scale, τ_2, is extracted from a fit of the data with an exponential form, Eq. (14), as shown by the inset. Snapshots on the right show that registration is not yet achieved at $t=\tau_1$.

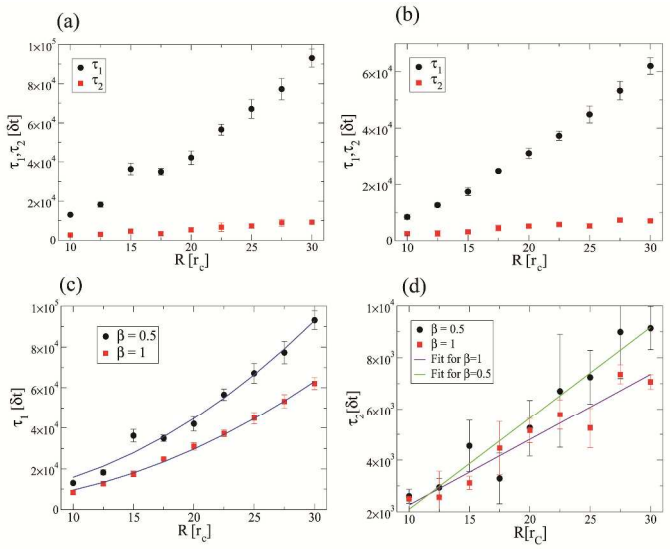

Fig. 5 (a,b) The relaxation times τ_1 and τ_2 as a function of domain radius R. (a) and (b) correspond to β=0.5 and β=0.5, respectively. (c) shows τ_1 vs. R for both values of β. The solid blue lines are fits with $A_0R^2+A_1$d. (d) shows τ_2 vs. R for both values of β. The solid lines are linear fits to the data.

This form of decay implies that the registration process is thermally driven at late times, when $\Delta h(t)$ is small. We note that the slow exponential decay at late times is not clearly discernable in Pantano *et al.*'s study [27]. It is noted, however, that the domain size in their work is about 4 nm, much smaller than the domain sizes in the present study.

The extracted time scales, τ_1 and τ_2, from fits of the data with Eqs. (13) and (14), are shown in Fig. 5 as a function of domain size for β=1and 0.5. Fig. 5(a) and (b) show that both time scales increase with increasing domain size, but that $\tau_1 >> \tau_2$, implying that the registration kinetics is dominated by the first regime. Fig. 5(c) shows that $\tau_1 \sim R^2$ for both values of β, which is in excellent agreement with Han-Haataja's prediction [28]. The large error bars in τ_2 vs. R make it difficult to accurately obtain its functional dependence on the domain size R. However, and as we will see in Sec. 3.3, our data is more consistent with $\tau_1 \sim R$, which implies that $\tau_2/\tau_1 \to 0$ as $R \to \infty$.

3.2 Effects of initial separation between domains

So far, presented results are based on simulations of domains, which are initially partially overlapped. A question that arises is whether an initial overlap is necessary in order to achieve registration. In order to test this, we performed simulations of domains with R=10r_c, β=0.5, and initially separated by $\Delta h(0)$=2R, 2.1R and 2.25R. Ten independent runs were performed for each case. Fig. 6 shows that in the case of a marginal initial overlap, i.e. for $\Delta h(0)$=2R, registration is observed in all of the 10 runs. However, while the registration kinetics begins at about t=0 in 7 runs, delays of different lengths are observed in 3 runs. This delay must be due to the Brownian motion of the domains centres of mass and to capillary fluctuations of the domains interfaces, driving the apposing domains away from overlap at the beginning. The same fluctuations can drive the domains closer to each other and eventual partial overlap. This is then followed by a registration process driven by interleaflet coupling. We note that independent of the delay time, the rate of the registration process is the same for all runs. This is expected since the registration rate should not depend on the value of the initial overlap, $\Delta h(0)$.

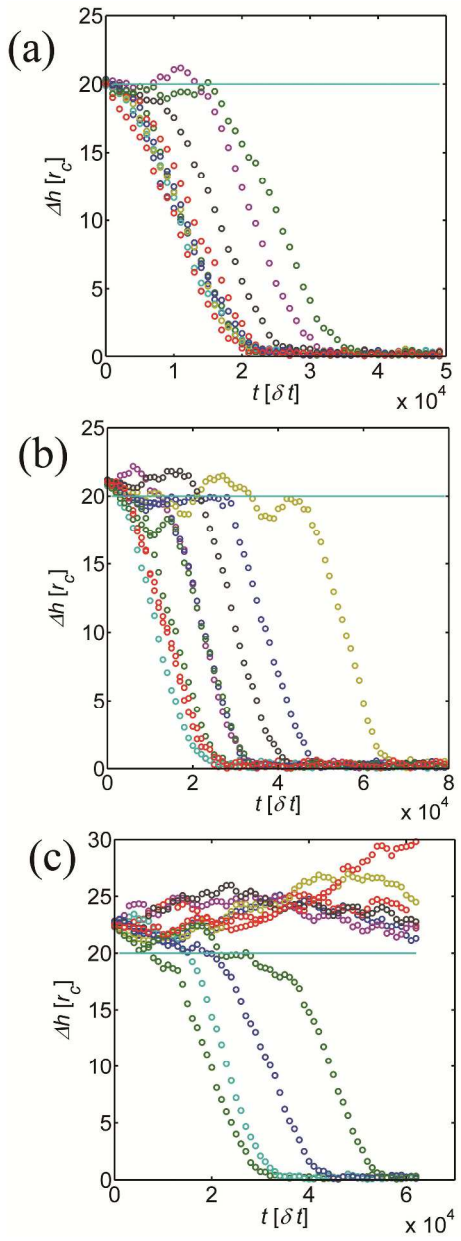

Fig. 6 Distance between the two domains centres of mass, $\Delta h(t)$ vs. time for different initial separations corresponding to $\Delta h(0)$=2R (a), 2,1R (b), and 2.25R (c). 10 independent runs are performed for each case. The solid lines correspond to the marginal distance between domains corresponding to 2R.

The simulation parameters are as follows: $L_x \times L_y \times L_z = (60\times60\times60)\ r_c^3$, $R = 10\ r_c$, and $\beta = 0.5$.

In the case of $\Delta h(0)=2.1R$, full registration is also observed in all 10 runs. However, registration begins at $t = 0$ in 3 runs only in this case, while a delay is observed in 7 runs. Finally in the case of $\Delta h(0)=2.25R$, which corresponds to a width of the non-overlap region equal to $2.5r_c$, registration occurs in 4 runs only. In this case, Brownian motion of the domains seems to drive them away from each other.

In Fig. 7, $\Delta h(t)$ and the number of interacting pairs, $N_{pairs}(t)$, of beads belonging to different domains are shown versus time for different initial separation distances. Fig. 7 shows a strong correlation between the onset of registration and the number of interacting pairs. In particular, as shown by Fig. 7(b and c), the initial plateau of $\Delta h(t)$ vs. time is correlated with no interacting pairs. This is particularly clearly demonstrated by Fig. 7(d) corresponding to a run for the case of $\Delta h(0)=2.25R$. The results of this section imply that some initial overlap between the domains is needed for registration to occur. Otherwise, registration may occur if domains experience some marginal overlap due to their Brownian motion and capillary fluctuations of their interfaces.

3.3 Effects of interleaflet coupling strength

In this section, we will discuss in more details the effect of the coupling strength on the relaxation time. We first show that the coupling strength, β, used in the present study is indeed proportional to the coupling strength, Λ, in Han-Haataja's theory [28]. The energy difference, ΔE, between the situation of an A-domain of radius R apposed to a B-domain of same size (Fig. 8(a)) and the situation of the A-domain in complete registration with an A-domain of same size (Fig. 8(b)) is given by

$$\Delta E = \pi R^2 \gamma \sim \pi R^2 \Lambda, \tag{15}$$

where γ is the interleaflet energy between A- and B-domains per unit of area. Within our framework, this energy difference is given by

$$\Delta E = \zeta \pi R^2 \left(a^{\perp}_{t_A t_B} - a_{t_A t_A} \right) \tag{16}$$

where ζ is a proportionality coefficient. Using Eq. (11), Eq. (16) then becomes

$$\Delta E = \zeta \pi R^2 \beta \left(a^{//}_{t_A t_B} - a_{t_A t_A} \right) \tag{17}$$

Eqs. (15) and (17) therefore imply that $\beta \sim \Lambda$.

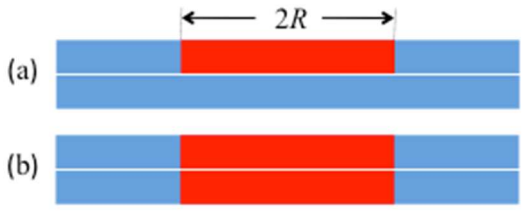

Fig. 8 Schematic illustration of (a) an A-domain (red) with radius R in the upper leaflet apposed to a lower leaflet composed of B-lipids (blue), and (b) an A-domain in the upper leaflet apposed to an A-domain in the lower leaflet.

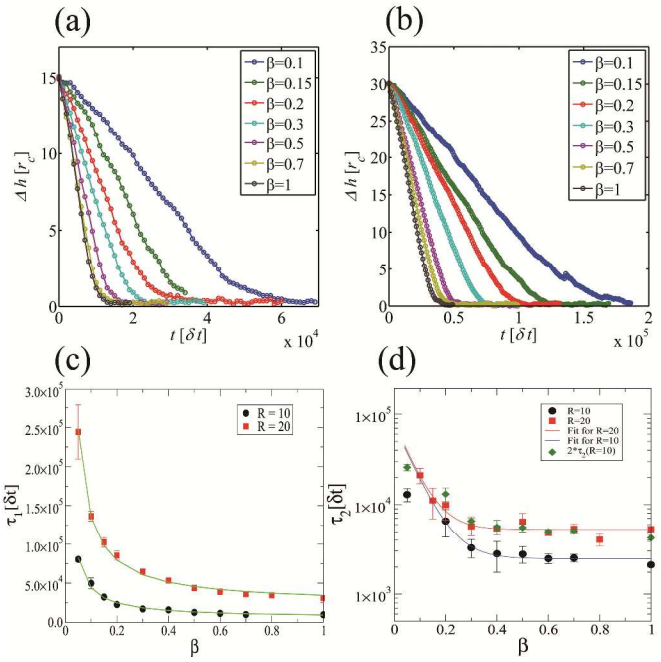

Fig. 9 (a) and (b) show the distance between the centers of mass of the two domains, Δh, vs. β for $R = 10r_c$ and $R = 20r_c$, respectively. (c) The time scale of the first regime, τ_1 vs. β for $R = 10r_c$ (solid circles), and 20 r_c (solid squares). The solid lines are fits with $A_0/\beta + A_1$, where A_0 and A_1 are integration constants. (d) The time scale of the first regime, τ_2 vs. β for $R = 10r_c$ (solid circles), and 20 r_c (solid squares). The solid lines are guides to the eye. The solid green diamonds correspond to $2\,\tau_2$ for the case of $R = 10r_c$. Notice the overlap of this with the data for $R = 20r_c$. All data here correspond to an initial separation $\Delta h(0)=1.5R$.

In Fig. 9, $\Delta h(t)$ vs. time is shown for $R=10r_c$ and $20r_c$ in the case of $\Delta h(0)=1.5R$ and for coupling strength, $0.1 < \beta < 1$. Figs. 9(a) and (b) show that the registration is slowed down when the interleaflet coupling is weakened. The extracted registration time scale during the first regime is found to decrease with β as $\tau_1 \sim 1/\beta$, as shown by Fig. 9(c), again in very good agreement with Han-Haataja's theory [28].

Fig. 9(d) shows that the extracted time scale τ_2, of the late-times exponential regime, also decreases with increasing β but then becomes independent of β for $\beta > 0.4$. The weaker dependence on β of τ_1 than that of τ_2 is attributed to the fact that the kinetics of registration during the first regime is dominated by the surface energy of the domains, as will be shown in the next subsection, which is strongly dependent on β (c.f. Fig. 9(a)), while the second regime kinetics is dominated by the line energy of the domains which is independent of β. Fig. 9(d) also shows that τ_2 for $R=20r_c$ is double that for $R=10r_c$ except for very small values of β. This implies that likely $\tau_2 \sim R$, which the previous Fig. 5(d) corroborates. Thus as the domains size becomes large, the first regime becomes dominant. We note that the apparent linear decay of Δh observed by Panatano

et al. simulations [27] might be to the lack of averaging. It is also expected that it becomes hard to distinguish between the linear and exponential regimes as $R \to 0$.

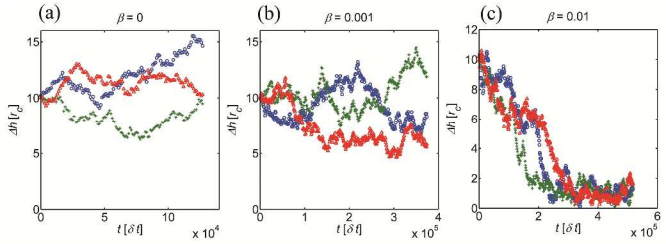

Fig. 10 Distance between two domains vs. time for different values of coupling strength. The simulation parameters are $R = 10r_c$, $\Delta h(0) = R$, and $L_x \times L_y \times L_z = (60 \times 60 \times 60) r_c^3$.

We also tested whether registration occurs for any positive value of the coupling β or if there is a finite small value of β below which no registration occurs. A series of additional simulations were performed for $\beta = 0$, 10^{-3}, and 10^{-2}, on systems With $R = 10r_c$ and $\Delta h(0) = R$. Results for $\Delta h(t)$ of three independent runs for each of the values of β are shown in Fig. 10. Fig. 10(a) shows that, as expected, no registration occurs for the case of no interleaflet coupling, $\beta = 0$. Fig. 10(b) shows that registration does not occur for finite, but very small values of the interleaflet coupling. However, registration occurs in all three runs when $\beta = 10^{-2}$, although in this case a good amount of random walk of the domains centres of mass occurs as demonstrated by the scattered data of each run. We note that Han-Haataja's theory, which ignores thermal fluctuations, predicts that registration occurs for any finite value of β [28].

3.4 Domains anisotropy during the registration kinetics

Fig. 2 shows that during the registration process, domains deviate from their circular shape and become elongated along the axis containing the centers of mass of the domains. In order to quantify this anisotropy, we calculated the ratio R_y/R_x where R_x and R_y are the extents of the domains along the x- and y-axis, respectively. In Fig. 11, the anisotropy ratio R_y/R_x is shown vs. time for the cases of $R = 15r_c$ and $R = 30r_c$, with $\beta = 1$. During the early stages of the registration process, R_y/R_x decreases with time from the value of 1 at $t = 0$, corresponding to a circle, to a value about 0.7, then increases with time towards 1 at later times. It is interesting to note that the decay in R_y/R_x occurs during the first regime during which $\Delta h(t)$ decay almost linearly with time. In contrast the increase of R_y/R_x, which corresponds to the restoration of the shape of the domains to circular shape, is more correlated with the exponential decay of $\Delta h(t)$. We note that the minimum of R_y/R_x is slightly lower for $R = 30r_c$ than for $R = 15r_c$, which implies that larger domains exhibit more anisotropy during the registration process than smaller ones. We note that in Han-Haataja's theory, domains are assumed to keep their circular shape during the kinetics [28].

In the following, we present a thermodynamic argument that we will use to explain the domains elongation during their registration process. We will use elliptical shape as a simple model for anisotropic domains, and show that the free energy of

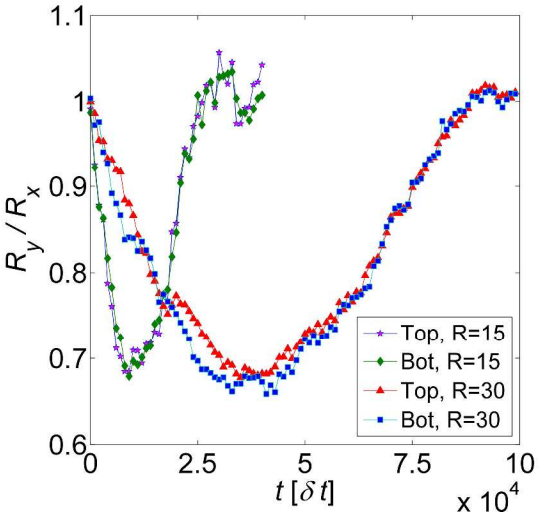

Fig. 11 Anisotropy parameter R_y/R_x vs. time in the case of $\beta = 1$. Purple and green symbols correspond to the upper and lower leaflets, respectively for $R = 15r_c$. Red and blue symbols correspond to the upper and lower leaflets, respectively for $R = 30r_c$.

two partially overlapping elliptical domains (see Fig. 12(b)) is smaller than that of two partially overlapping circular domains of same size and separated by the same distance (see Fig. 12(a)). Let λ be the line tension and σ be the interlayer surface tension between A and B-domains. The free energy of two equal sizes, partially overlapping elliptical domains with semi-major and semi-minor axes given by R_x and R_y and (see Fig. 12), respectively, and separated by a distance Δh, is given by [38],

$$F_{\text{ellipse}} \cong 2\lambda\pi\left[\frac{3}{2}\left(R_x + R_y\right) - \sqrt{R_x R_y}\right] + 4\sigma R_x R_y\left[\frac{\pi}{2} - \arcsin\left(\sqrt{1-\left(\frac{\Delta h}{2R_x}\right)^2}\right) + \frac{\Delta h}{2R_x}\sqrt{1-\left(\frac{\Delta h}{2R_x}\right)^2}\right]. \quad (18)$$

where the first term accounts for the line energy of the elliptical domains, and the second term accounts for excess surface energy due to the non-overlapping areas of the domains. In comparison, the excess free energy of two partially overlapping circular domains of radius R and separated by the same distance, Δh, is given by,

$$F_{cir} = 4\pi R\lambda + 4\sigma R^2\left[\frac{\pi}{2} - \arcsin\left(\sqrt{1-\left(\frac{\Delta h}{2R}\right)^2}\right) + \frac{\Delta h}{2R}\sqrt{1-\left(\frac{\Delta h}{2R}\right)^2}\right], \quad (19)$$

with the condition $R^2 = R_x R_y$.

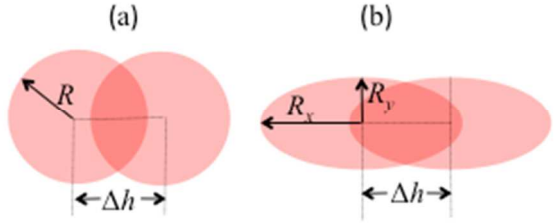

Fig. 12 (a) shows two partially overlapping circular domains of radius R and separated by distance Δh. (b) shows two partially overlapping elliptical domains with semi-major axis, R_x, and semi-minor axis, R_y, and separated by distance Δh.

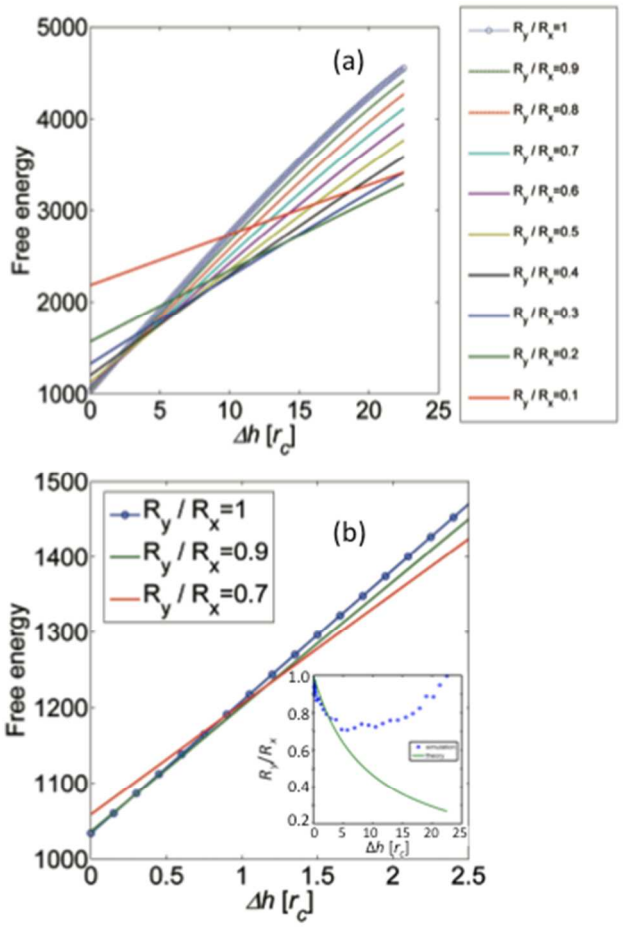

Fig. 13 Free energy of partially overlapping elliptical domains vs. Δh for varying anisotropy parameter R_y/R_x. Parameters used are $R=15r_c$, $\lambda=5.5\varepsilon/r_c$, and $\sigma=2.9\varepsilon/r_c^2$. (b) shows the free energy shown in (a) for small values of Δh. The inset in (b) shows a comparison between simulation and thermodynamic arguments of the anisotropy parameter R_y/R_x vs. Δh.

The free energy of the elliptical domains versus the distance separating them, Δh, for the case of $R=15r_c$ is shown systematically in Fig. 13(a), for values of the anisotropy parameter, R_y/R_x, varying between 0.1 and 1. This figure shows that for a separation $\Delta h=22.5\ r_c$, the free energy of circular domains is higher than that of any elliptical domains, and that domains with R_y/R_x between 0.1 and 0.2, have a minimum free energy for $\Delta h=22.5\ r_c$. This is due to the fact that the increase in line energy, due to the increased perimeters of elliptical domains, is compensated by an increase in overlap area and therefore a decrease in the non-overlapping areas.

As the distance between domains is decreased, i.e., as time proceeds, the free energy is minimized for higher values of R_y/R_x, implying that anisotropy is reduced as time proceeds. In particular, Fig. 13(b) shows that circular domains become energetically favourable only in the limit of very small domains separation ($\Delta h < r_c$). Therefore, the thermodynamic arguments above imply that during the registration process, where Δh decreases with time, the domains anisotropy should decrease with increasing time, until a full overlap of circularly shaped domains is achieved. We note that this thermodynamic argument assumes that the registration kinetics is slow enough to allow domains to attain their equilibrium shape. The thermodynamic arguments above imply that the first regime, which is characterized by an almost linear decay in Δh is dominated by the surface energy of the two domains, while the second regime, characterized by an exponential decay of Δh is dominated by the line energy of the domains.

In the inset of Fig. 13(b), R_y/R_x determined from the thermodynamic arguments (solid line) and simulation (circles) is plotted versus Δh. This figure shows that for small Δh (corresponding to late times), the simulation data almost coincides with that obtained from the thermodynamic arguments. However, a strong deviation is observed between the simulation data and the theoretical arguments for large values of Δh (early times). The first reason for this discrepancy is that the simulations starts with circular domains, and the domains, and during early times, the domains do not have enough time to equilibrate their shape while moving closer to each other. The second reason for this discrepancy could be due to the fact that the domains in our simulations are in fact not elliptical, as demonstrated by the snapshots of Fig. 2.

Very recently, Han *et al.* [39] investigated the effect of hydrodynamic interaction on the kinetics of registration. In particular, they found that the domains undergo elongation during the process of registration if the kinetics is dominated by membrane viscosity. In contrast, domains remain circular if the kinetics is dominated by interleaflet friction. A numerical test

of this Han et al.'s theory requires a systematic manipulation of both the membrane hydrodynamic drag and the interleaflet friction. However, many of the membrane parameters are inter-related, making it difficult to perform such a test.

4 Summary and concluding remarks

In this article, we presented results of a systematic computational investigation of the kinetics of domain registration in self-assembled multicomponent lipid bilayers using dissipative particle dynamics. Our main results are that the kinetics of registration proceeds through two main regimes. During the first regime, the distance between the centres of mass of the apposing domains, Δh, decrease almost linearly with time, in very good agreement with the recent theory of Han and Haataja [28]. The second regime is characterized by an exponential time decay of Δh. The time scales of both regimes are found to increase with increasing the domain size and decreasing the interleaflet coupling. In particular, we found that the time scale of the first regime, $\tau \sim R^2/\beta$, where R and β are the domain size and interleaflet coupling, in very good agreement with Han-Haataja's theory [28]. We also found that some overlap between domains is needed for registration to occur. Otherwise, registration may occur as a result of Brownian motion of initially non-overlapping domains. A quantitative comparison between our simulation results and Han-Haataja theory is difficult due to the fact that several parameters that enter the registration time scale cannot easily be extracted from the simulation. In particular, the interleaflet friction coefficient and the lipid bilayer's inplane viscosity cannot be extracted. Furthermore, some of the parameters are interdependent. For example, the interleaflet friction coefficient and the interlaflet cupling strength should be related, and therefore cannot be varied independently.

During the process of registration, domains are stretched along the direction separating their centres of mass. Their anisotropy parameter, defined as the ratio between their minor and major axes, R_y/R_x, initially decreases with time from 1 to a value about 0.7 then increases back to 1 at later times. The anisotropy generated by registration kinetics is the result of competition between the domains line energy and surface energy between unlike domains.

As mentioned earlier, domains in lipid membranes are almost always registered. This can be understood using the following argument: Consider a multicomponent membrane undergoing phase separation kinetics, as a result of their Brownian motion and coalescence, the average domain grows as $R \sim t^{1/3}$ [20,21]. Partial overlap between domains in the apposing leaflets will lead to their quick registration with a time scale $t_{reg} \sim R^2$, which is less than the coalescence time scale. Therefore, domains undergo registration during the early stages of the phase separation process, making it almost impossible to see large non-overlapping domains.

Acknowledgements

M.L. acknowledges the financial support from the National Science Foundation (DMR-0812470) and the National Institute of General Medical Sciences of NIH (R15GM106326). K.S. is funded by the Development Promotion of Science and Technology, Thailand. C.M. is supported by the Centre of Excellence in Mathematics, Thailand. The content is solely the responsibility of the authors and does not necessarily represent the official views of the National Institutes of Health.

Notes and references

[a]*Department of Physics, The University of Memphis, Memphis, TN 38152, USA, E-mail: mlaradji@memphis.edu*
[b]*Department of Physics, Mahidol University, Bangkok 10400, Thailand*
[c]*Department of Chemistry, Mahidol University, Bangkok 10400, Thailand*
[d]*Institute of Innovative Learning, Mahidol University, Bangkok 10400, Thailand*
[e]*Department of Physics, Indian Institute of Technlogy Madras, Chenna 600036, India*
[f]*MEMPHYS-Center for Biomembrane Physics, University of Southern Denmark, 5230 Odense, Denmark*

1. C. Dietrich, L.A. Bagatolli, Z.N. Volovyk, N.L. Thompson NL, M. Levi, K. Jacobson and E. Gratton, *Biophys. J.*, 2001, **80**, 1417-1428.
2. S.L. Veatch and S.L. Keller, *Phys. Rev. Lett.*, 2002, **89**, 268101.
3. T. Baumgart, S.T. Hess and W.W. Webb, *Nature (London)*, 2003, **425**, 821-824.
4. S.L. Veatch and S.L. Keller *Biophys. J.*, 2003, **85**, 3074-3083.
5. S.L. Veatch and S.L. Keller, *Biochim. Biophys. Acta – Mol. Cell Res.*, 2005, **1746**, 172-185.
6. L. Li, X. Liang, M. Lin and Y. Wang, *J. Am. Chem. Soc.*, 2005, **127**, 17996-17997.
7. M. Yanagisawa, M. Imai, T. Masui, S. Komura and T. Ohta, *Biophys. J*, 2007, **92**, 115-125.
8. X. Liang, L. Li, F. Qiu and Y. Yang, *Physica A*, 2010, **389**, 3965-3971.
9. M.D. Collins and S.L. Keller, *Proc. Nat. Acad. Sci.*, 2008, **105**, 124-128.
10. K. Simons and G. van Meer G, *Biochem.*, 1988, **27**, 6197-6202.
11. L. Pike, *J. Lipid Res.*, 2009, **50**, S323-S328.
12. K. Simons and J.L. Sampaio, *Cold Spring Harb. Perspect. Biol.*, 2011, **3**, a004697.
13. M.D. Collins, *Biophys. J.*, 2008, **94**, L32-L34.
14. S. May, *Soft Matter*, 2009, **5**, 3148-3156.
15. P.F. Devaux and A. Zachowski, *Chem. Phys. Lipid,* 1994, **73**,107-120.
16. T.Y. Wang and J.R. Silvius, *Biophys. J.,* 2001, **81**, 2762-2773.
17. K. Simons and D. Toomre, *Nat. Rev. Mol. Cell Biol.,* 2001, **1**, 31-39.
18. S. Yamamoto, Y. Maruyama and S-a. Hyodo S-a, *J. Chem. Phys.*, 2002, **116**, 5842.
19. S. Yamamoto and S-a. Hyodo, *J. Chem. Phys.*, 2003, **118**, 7937.
20. M. Laradji and P.B. Sunil Kumar, *Phys. Rev. Lett.*, 2004, **93**, 198105.

21. M. Laradji and P.B. Sunil Kumar, *J. Chem. Phys.,* 2005, **123**, 224902.
22. K. Sornbundit, C. Modchang, W. Triampo, D. Triampo D and N. Nuttavut, *Euro. Phys. J. Appl. Phys.*, 2013, **64**, 11101.
23. H.J. Risselada and S.J. Marrink, *Proc. Nat. Acad. Sci.*, 2008, **105**, 17367-17372.
24. J. Fan, T. Han, and M. Haataja, *J. Chem. Phys*., 2010, **133**, 235101.
25. B.A. Camley and F.L.H. Brown, *J. Chem. Phys*., 2011, **135**, 225106.
26. M. Laradji and P.B. Sunil Kumar, *Adv. Planar Lipid Bilayers and Liposomes,* 2011, **14**, 201-233.
27. D.A. Pantano, P.B. Moore, M.L. Klein and D.E. Discher, *Soft Matter*, 2011, **7**, 8182-8191.
28. T. Han and M. Haataja, *Soft Matter*, 2013, **9**, 2120-2124.
29. K. Elder, M. Grant, N. Provatas and J.Kosterlitz, *Phys. Rev. E*, 2001, **64**, 021604.
30. T. Han and M. Haataja, *Phys. Rev. E,* 2011, **84**, 051903.
31. P.J. Hoogerbrugge and J.M.V.A. Koelman, *Europhys. Lett.,* 1992, **19**, 155.
32. P. Español and P.B. Warren, *Europhys. Lett.* 1995, **30**, 191.
33. P. Español, *Europhys. Lett.*, 1997, **40**, 631.
34. R.D. Groot and P.B. Warren, *J. Chem. Phys.* 1997, **107**, 4423.
35. M. Kranenburg, M. Venturoli and B. Smit, *Phys. Rev. E*., 2003, **7**, 060901(R).
36. G. Besold, I. Vattulainen, M. Karttunen and J.M. Polson, *Phys. Rev. E,* 2000, **62**, R7611.
37. P. Nikunen, M. Karttunen and I. Vattulainen, *Comp. Phys. Comm.*, 2003, **153**, 407-423.
38. I.N. Bronshtein and K.A. Semendyayev, *Handbook of mathematics*, Van Nostrand Reinhold, New York, 1985.
39. T. Han, T.P. Bailey, and M. Haataja, *Phys. Rev. E*, 2014, **89**, 032717.

